Sensors and Materials, Vol. 36, No. 2 (2024) 489–497
MYU Tokyo

S & M 3536

Photoluminescence and Scintillation Properties of Ce-doped $BaHfO_3$ Crystals

Hiroyuki Fukushima,[1*] Daisuke Nakauchi,[2] Takumi Kato,[2]
Noriaki Kawaguchi,[2] and Takayuki Yanagida[2]

[1]Department of Electrical and Electronic Engineering, National Institute of Technology, Fukui College, Geshi, Sabae, Fukui 916-8507, Japan
[2]Division of Materials Science, Nara Institute of Science and Technology, 8916-5 Takayama-cho, Ikoma, Nara 630-0192, Japan

(Received October 31, 2023; accepted January 22, 2024)

Keywords: scintillation, photoluminescence, $BaHfO_3$, floating zone

The photoluminescence (PL) and scintillation properties of Ce-doped $BaHfO_3$ crystals were investigated. The Ce-doped $BaHfO_3$ crystal is transparent and colorless after annealing treatment under a reduction condition. The broad luminescence band at ~370 nm was observed under ~280 nm excitation with the decay time of ~17 ns. The X-ray-induced scintillation spectra also showed the broad luminescence band at ~380 nm with a fast decay. The origin of the broad luminescence band at ~380 nm is attributed to the 5d–4f transition of Ce^{3+}. The pulse height distribution under ^{137}Cs gamma ray irradiation using Ce-doped $BaHfO_3$ exhibited a distinguishable photoabsorption peak. The light yield of Ce-doped $BaHfO_3$ is ~1600 photons/MeV.

1. Introduction

Ionizing radiation detection is conducted by two measurement methods. One is a direct measurement using, for example, a Ge semiconductor detector. The other is an indirect measurement using, for example, a scintillation detector. A scintillation detector uses a scintillator, which generates luminescence under ionizing radiation irradiation. The generated luminescence is detected by a photodetector such as a photomultiplier tube (PMT) and a photodiode. For example, X-ray images are taken using a scintillation detector,[(1)] and positron emission tomography also uses many scintillators.[(2)] The typically required properties for scintillators are a high light yield and a fast decay time. Moreover, there are some requirements for density and effective atomic number for some applications. In particular, a high density and effective atomic number of materials are important for the detection of X- and gamma rays.[(3)] Scintillators with a fast decay are realized by luminescence from the 5d–4f transition of Ce^{3+} or Pr^{3+}.[(4)] Thus, scintillation properties have been investigated in Ce- or Pr-doped dense materials to develop a novel X- or gamma-ray scintillator.[(5–12)] Moreover, the scintillation properties of

*Corresponding author: e-mail: fukushima@fukui-nct.ac.jp
https://doi.org/10.18494/SAM4762

ISSN 0914-4935
https://myukk.org/

many materials such as single crystals,[13–22] ceramics,[23–27] and glasses[28–37] have been investigated.

MHfO$_3$ (M = Ca, Sr, or Ba) have high density and effective atomic number. The scintillation properties of many Ce-doped MHfO$_3$ have been investigated.[38–42] The light yield of a Ce-doped CaHfO$_3$ single crystal, which has a density of 6.9 g/cm^3, is ~7800 photons/MeV with a fast decay of ~22 ns.[43] The light yield of Ce-doped CaHfO$_3$ is increased by Mg substitution.[44] The density of a SrHfO$_3$ single crystal is 7.6 g/cm^3, and the light yield is ~400 photons/MeV.[45] BaHfO$_3$ has the highest density of 8.3 g/cm^3 among the MHfO$_3$ series. The scintillation properties of Ce-doped BaHfO$_3$ transparent ceramics have been investigated.[46] In this work, the integrated light yield was investigated; however, there is no report on the light yield of Ce-doped BaHfO$_3$ determined from the pulse height distribution.

In this study, Ce-doped BaHfO$_3$ crystals were synthesized by the floating zone (FZ) method, and the photoluminescence (PL) and X-ray-induced scintillation spectra and decay curves were measured. Finally, the pulse height distribution under ^{137}Cs gamma-ray irradiation was investigated to estimate the quantitative light yield of Ce-doped BaHfO$_3$.

2. Materials and Methods

Ce-doped BaHfO$_3$ crystals were synthesized by the FZ method. Four xenon lamps as a heating source were installed in the FZ instrument. The details of the equipment are found in Ref. 47. The feed rods were synthesized by a simple sintering method. The starting materials, namely, BaCO$_3$ (99.99%, Rera Metallic), HfO$_2$ (99.95%, Furuuchi Chemical), and CeO$_2$ (99.99%, Furuuchi Chemical), were mixed using a mortar and pestle. The mixed powder was sintered at 1200 °C for 8 h. The sintered powder was remixed and further sintered at 1400 °C for 8 h. The resintered powder was hydrostatically pressed into a cylindrical rod and again sintered at 1500 °C for 8 h. The amount of BaCO$_3$ in this powder was increased by 30% from the stoichiometric composition of BaHfO$_3$ to compensate for the volatilization of Ba during the crystal growth. The pulling-down rate was 50 mm/h, and the rotation rates of the upper and lower shafts were 28 and 25 rpm, respectively. The synthesized crystals were treated under a reduction atmosphere to suppress the formation of Ce^{4+} ions. The crystals were put into graphite powder under vacuum. The heating temperature was 800 °C, and the treatment time was 96–144 h. The treatment time was determined on the basis of the appearance of the samples.

The measurement range of the X-ray diffraction (XRD) patterns was 2θ = 10 to 70 degrees (Rigaku, Miniflex600), and the X-ray source was CuKα. The PL excitation and emission map and quantum yield (QY) were measured using the Hamamatsu Photonics C11347 spectrometer. The PL decay curves were also measured using the Hamamatsu Photonics C11367 spectrometer. The X-ray-induced scintillation spectra, decay curves, and afterglow curves were measured with original setups.[48,49] The voltage and current applied to the X-ray tube for the scintillation spectra were 40 kV and 1.2 mA, respectively. The pulse height distribution under ^{137}Cs gamma-ray irradiation was measured using a laboratory-made setup.[48] The PMT used was of the ultra–bi-alkali type (Hamamatsu Photonics, R7600-200).

3. Results and Discussion

A photograph of the synthesized samples is shown in Fig. 1. The as-synthesized samples were brown. The 1 and 5% samples were transparent, and the 0.3 and 3% samples were opaque. The 0.3 and 1% samples were black because some graphite powders were inside the sample. The 3% sample was also partially black for the same reason. The 5% sample was orange. The as-synthesized sample was brown; thus, the treatment time or temperature of the 5% sample was insufficient compared with those of the other samples. To investigate the absorption wavelength, diffuse transmission spectra were measured, and the results are shown in Fig. 2. Absorption bands were observed at ~250 and 300 nm in all the samples. In contrast, the 5% sample showed a deep absorption band at ~450–550 nm compared with the 1% sample. The 5% sample was orange, as shown in Fig. 1, because the absorption band was at ~450–550 nm. The transmittance of the 0.3% sample was the lowest among the samples, and the black color contributes to the low transmittance.

Figure 3 shows the XRD patterns of the synthesized samples and references. All the samples included $BaHfO_3$ (ICDD. 24-0102) and monoclinic HfO_2 (COD. 9013470). The melting point of $BaHfO_3$ is quite high, and the vapor pressure of Ba is also high; thus, Ba was volatilized during crystal synthesis, and HfO_2 remained in the samples. The XRD peak position did not seem to shift. The ionic radii of Ba^{2+} (1.61 Å in twelve-coordination), Hf^{4+} (0.71 Å in six-coordination), Ce^{3+} (1.34 Å in twelve-coordination and 1.01 Å in six-coordination), and Ce^{4+} (1.14 Å in twelve-coordination and 0.87 Å in six-coordination) are not the same in the same coordination number.[50] The doped Ce ions were considered to be incorporated into the Ba or Hf sites; thus, the peak shift was quite small.

Figure 4 shows the PL excitation and emission map of the 1% sample as the representative sample because the other samples also exhibit similar spectra but with a different intensity, and

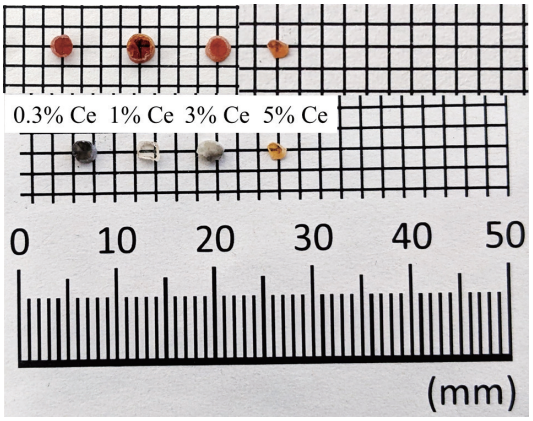

Fig. 1. (Color online) Photograph of as-synthesized (top) and treated Ce-doped $BaHfO_3$ samples (bottom).

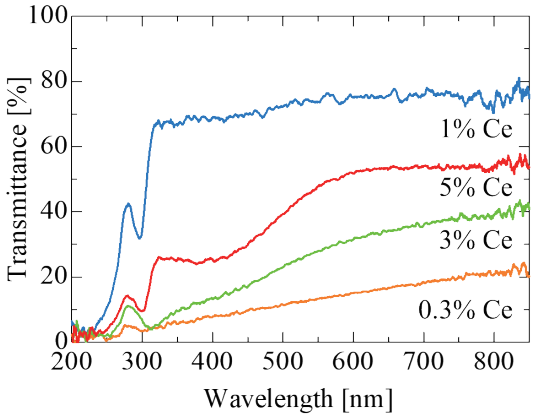

Fig. 2. (Color online) Diffuse transmission spectra of Ce-doped $BaHfO_3$ samples.

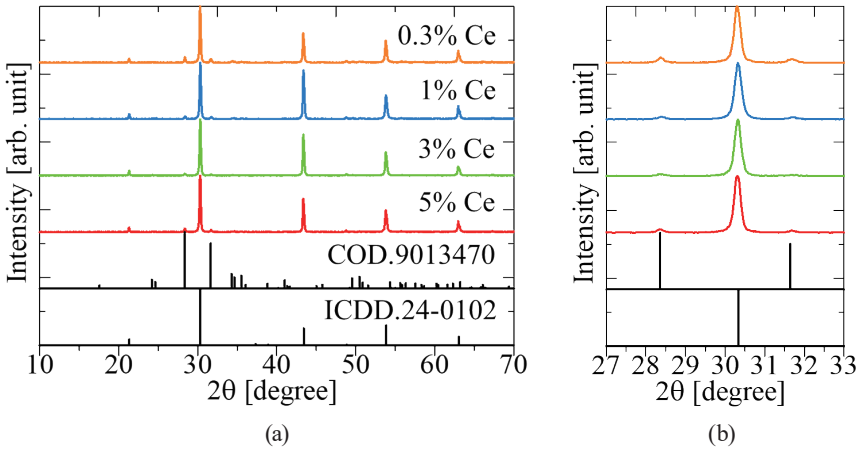

Fig. 3. (Color online) (a) XRD patterns of Ce-doped $BaHfO_3$ samples and references and (b) enlarged XRD patterns from $2\theta = 27$ to 33 degrees.

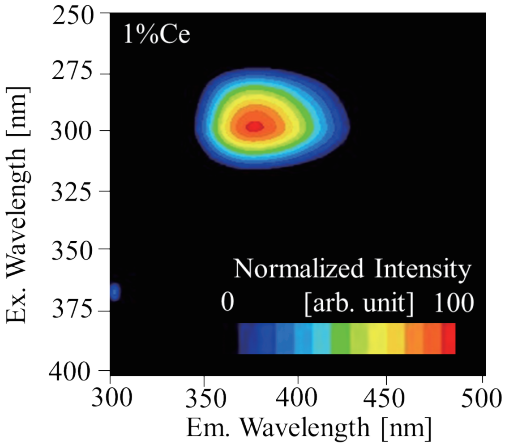

Fig. 4. (Color online) PL excitation and emission map of 1% Ce-doped $BaHfO_3$ sample.

the as-synthesized samples showed a rather low luminescence intensity. The horizontal and vertical axes are emission and excitation wavelengths, respectively. All the samples exhibited the broad luminescence band at ~370 nm under the excitation wavelength of ~300 nm. These emission and excitation wavelengths were similar to those in previously reported results of Ce-doped $BaHfO_3$.[41,51] The PL *QY*s were 11.6% for the 0.3% sample, 30.5% for the 1% sample, 18.0% for the 3% sample, and 11.8% for the 5% sample. The highest PL *QY* was observed in the 1% sample, which was colorless compared with the same sample before treatment. The brownish color is attributed to Ce^{4+}.[52] The sample treatment was conducted to suppress the formation of Ce^{4+} ions because Ce^{4+} ions do not contribute to the luminescence. Thus, the colorless or white sample involved less Ce^{4+} ions and emitted luminescence due to the 5d–4f transition of Ce^{3+}, leading to an increase in the PL *QY*.

Figure 5 shows the PL decay curves of Ce-doped $BaHfO_3$. The excitation and monitoring wavelengths were 280 and 370 nm, respectively. The decay curves were fitted by one exponential function. The obtained PL decay time is listed in Table 1. The PL decay time of ~17 ns was faster

than the typical decay time due to the 5d–4f transition of Ce^{3+}. For example, the decay times were ~60 ns (Ce-doped Gd_2SiO_5),[53] ~40 ns (Ce-doped Lu_2SiO_5),[54] and ~100 ns (Ce-doped $Y_3Al_5O_{12}$).[55] In contrast, the decay time of Ce-doped $YAlO_3$ and $LuAlO_3$ was ~17 ns.[4] Shorter wavelengths and higher refractive indices are associated with faster decay times. The emission wavelength of Ce-doped $BaHfO_3$ was relatively short, and the refractive index was greater than 2.[56] Therefore, the decay time of Ce-doped $BaHfO_3$ was fast.

Figure 6 shows the X-ray-induced scintillation spectra of Ce-doped $BaHfO_3$. The peak wavelength was ~380 nm, which was slightly shifted to a longer wavelength compared with the PL emission peak. The measurement geometry of X-ray-induced scintillation spectra was of the transmission type. In contrast, the PL spectrum measurement was conducted in the reflection-type geometry. Thus, the scintillation light was absorbed by the sample, and the peak wavelength was shifted to a longer wavelength.

Figure 7 shows the X-ray-induced scintillation decay curves of Ce-doped $BaHfO_3$. The observed decay curves contained fast and slow decay components. The obtained decay time is

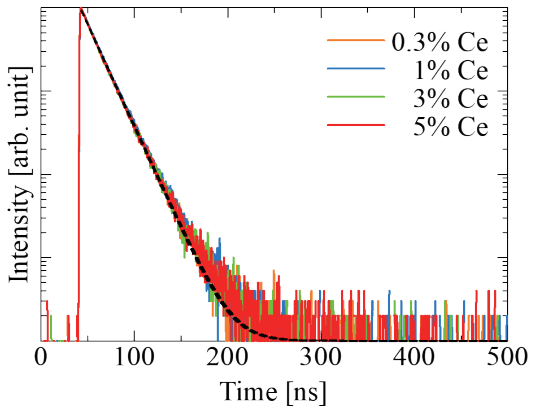

Fig. 5. (Color online) PL decay curves of Ce-doped $BaHfO_3$ samples.

Table 1
PL and scintillation decay times of Ce-doped $BaHfO_3$.

Sample	PL decay time	Scintillation decay time	
	τ^1 (ns)	τ^1 (ns)	τ^2 (ns)
0.3% Ce	17	18 (96.3%)	375 (3.7%)
1% Ce	17	16 (96.3%)	241 (3.7%)
3% Ce	17	14 (98.4%)	352 (1.6%)
5% Ce	17	15 (96.6%)	343 (3.4%)

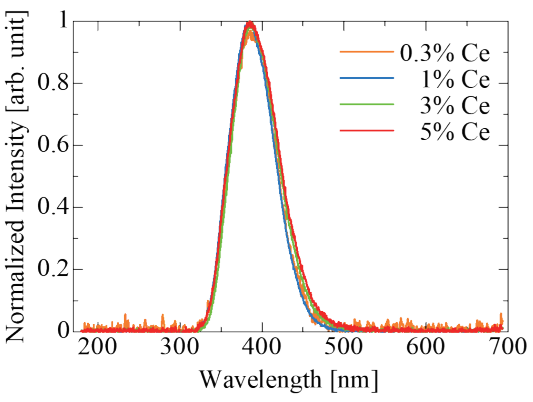

Fig. 6. (Color online) X-ray-induced scintillation spectra of Ce-doped $BaHfO_3$ samples.

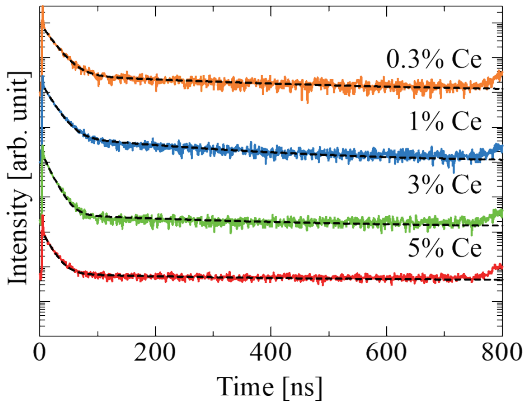

Fig. 7. (Color online) X-ray-induced scintillation decay curves of Ce-doped $BaHfO_3$ samples.

listed in Table 1. The fast decay time was ~14–18 ns, which was close to those in PL decay. The origin of the fast decay was attributed to the 5d–4f transition of Ce^{3+} owing to the decay time, the broad emission band, and the emission wavelength, as shown in Fig. 5. The slow decay was typically observed in the Ce-doped MHfO$_3$ (M = Ca and Sr) series,[38,43,44,57] and the origin was attributed to some types of defect.

Figure 8 shows the afterglow curves of Ce-doped $BaHfO_3$. The afterglow level is defined as the ratio of the intensity at 20 ms after stopping X-ray exposure to the intensity during X-ray exposure. The afterglow levels of the 0.3, 1, 3, and 5% samples were 1550, 420, 1040, and 860 ppm, respectively. These afterglow levels were lower than those in the Ce-doped MHfO$_3$ series.[38,43,45]

Figure 9 shows the pulse height distribution of the ^{137}Cs gamma ray using Ce-doped $BaHfO_3$ and $Bi_4Ge_3O_{12}$ (BGO). The 1 and 3% samples exhibited a discriminable peak due to photoabsorption. The light yields of the 1 and 3% samples were 1600 and 1300 photons/MeV, respectively, compared with the peak position of BGO (6800 photons/MeV) and the quantum efficiency of PMT. Although the 3% sample had a black region on the sample surface, the peak was observed. Thus, the black region did not affect the results of the pulse height distribution. The reported integrated light yield of Ce-doped $BaHfO_3$ was ~40000 photons/MeV.[46] The integrated light yield is estimated on the basis of the integrated intensity of the scintillation spectrum compared with a reference and a sample. The integrated light yield depends on not only the light yield, but also the stopping power of materials.[58] Thus, we must evaluate the light yield using the pulse height distribution. The light yield of the present Ce-doped $BaHfO_3$ was more than 10 times lower than the previous result.[46]

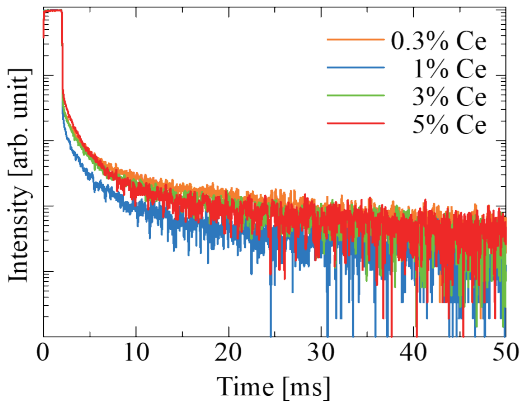

Fig. 8. (Color online) Afterglow curves of Ce-doped $BaHfO_3$ samples.

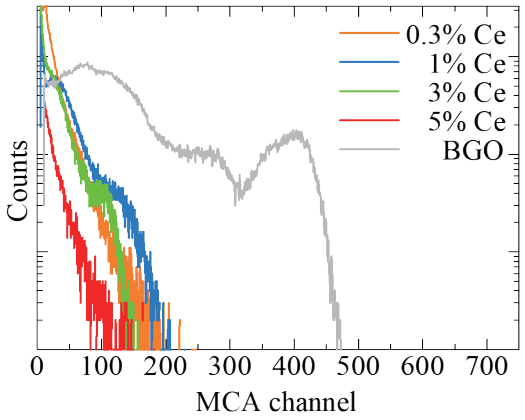

Fig. 9. (Color online) Pulse height distribution of ^{137}Cs gamma ray using Ce-doped $BaHfO_3$ samples.

4. Conclusions

The PL and scintillation properties of Ce-doped $BaHfO_3$ were investigated. The synthesized samples contained not only the $BaHfO_3$ phase but also the monoclinic HfO_2 phase. The as-synthesized $BaHfO_3$ showed low emission intensity. After the annealing treatment under the reduction condition, the emission intensity and the PL *QY* increased. The 1% sample exhibited the highest PL *QY* of 30.5% among the samples. The broad luminescence band at ~370–380 nm was observed in PL and scintillation. The PL and scintillation decay curves showed a fast decay of ~17 ns and a slow decay of ~241–375 ns. Ce-doped $BaHfO_3$ crystals exhibited a photoabsorption peak under ^{137}Cs gamma-ray irradiation, and the maximum light yield was 1600 photons/MeV. The Ce-doped $MHfO_3$ (*M* = Ca, Sr, and Ba) showed blue luminescence and fast decay under X-ray irradiation. The light yield of Ce-doped $BaHfO_3$ is lower than that of Ce-doped $CaHfO_3$,[43] but higher than that of Ce-doped $SrHfO_3$.[45]

Acknowledgments

This work was supported by a Grant-in-Aid for Scientific Research A (22H00309), Grants-in-Aid for Scientific Research B (22H03872, 22H02939, 21H03733, and 21H03736), Early-Career Scientists (23K13689), and Challenging Exploratory Research (22K18997) from the Japan Society for the Promotion of Science. The Cooperative Research Project of the Research Center for Biomedical Engineering, A-STEP (JPMJTM22DN) from JST, Kazuchika Okura Memorial Foundation, Asahi Glass Foundation, Nakatani Foundation, and Konica Minolta Science and Technology Foundation are also acknowledged.

References

1 H. Nanto: Sens. Mater. **30** (2018) 327. https://doi.org/10.18494/SAM.2018.1803
2 C. L. Melcher: J. Nucl. Med. **41** (2000) 1051.
3 T. Yanagida, T. Kato, D. Nakauchi, and N. Kawaguchi: Jpn. J. Appl. Phys. **62** (2022) 10508. https://doi.org/10.35848/1347-4065/ac9026
4 P. Dorenbos: IEEE Trans. Nucl. Sci. **57** (2010) 1162. https://doi.org/10.1109/TNS.2009.2031140
5 D. Nakauchi, H. Fukushima, T. Kato, N. Kawaguchi, and T. Yanagida: Sens. Mater. **34** (2022) 611. https://doi.org/10.18494/SAM3696
6 T. Yanagida, T. Kato, D. Nakauchi, and N. Kawaguchi: Sens. Mater. **34** (2022) 595. https://doi.org/10.18494/SAM3684
7 P. Kantuptim, M. Akatsuka, D. Nakauchi, T. Kato, N. Kawaguchi, and T. Yanagida: Sens. Mater. **32** (2020) 1357. https://doi.org/10.18494/SAM.2020.2726
8 Y. Shao, R. L. Conner, N. R. S. Souza, R. S. Silva, and L. G. Jacobsohn: Jpn. J. Appl. Phys. **62** (2023) 010601. https://doi.org/10.35848/1347-4065/ac9941
9 R. Nakamori, N. Kawano, A. Takaku, D. Onoda, Y. Takebuchi, H. Fukushima, T. Kato, K. Shinozaki, and T. Yanagida: Sens. Mater. **34** (2022) 707. https://doi.org/10.18494/SAM3689
10 G. Ito, H. Kimura, D. Shiratori, D. Nakauchi, T. Kato, N. Kawaguchi, and T. Yanagida: Sens. Mater. **34** (2022) 685. https://doi.org/10.18494/SAM3681
11 M. Koshimizu, Y. Fujimoto, and K. Asai: Sens. Mater. **35** (2023) 521. https://doi.org/10.18494/SAM4149
12 Y. Fujimoto, D. Nakauchi, T. Yanagida, M. Koshimizu, and K. Asai: Sens. Mater. **34** (2022) 629. https://doi.org/10.18494/SAM3693
13 Y. Takebuchi, T. Kato, D. Nakauchi, N. Kawaguchi, and T. Yanagida: Sens. Mater. **34** (2022) 645. https://doi.org/10.18494/SAM3685

14 M. Akatsuka, N. Daisuke, K. Takumi, N. Kawaguchi, and T. Yanagida: Sens. Mater. **34** (2022) 619. https://doi.org/10.18494/SAM3692
15 P. Kantuptim, D. Nakauchi, T. Kato, N. Kawaguchi, and T. Yanagida: Sens. Mater. **34** (2022) 603. https://doi.org/10.18494/SAM3690
16 P. Kantuptim, T. Kato, D. Nakauchi, N. Kawaguchi, and T. Yanagida: Crystals **12** (2022) 459. https://doi.org/10.3390/cryst12040459
17 K. Okazaki, D. Onoda, D. Nakauchi, N. Kawano, H. Fukushima, T. Kato, N. Kawaguchi, and T. Yanagida: Sens. Mater. **34** (2022) 575. https://doi.org/10.18494/SAM3678
18 D. Onoda, M. Akatsuka, N. Kawano, T. Kato, D. Nakauchi, N. Kawaguchi, and T. Yanagida: Sens. Mater. **34** (2022) 585. https://doi.org/10.18494/SAM3679
19 D. Shiratori, H. Fukushima, D. Nakauchi, T. Kato, N. Kawaguchi, and T. Yanagida: Sens. Mater. **35** (2023) 439. https://doi.org/10.18494/SAM4140
20 P. Kantuptim, T. Kato, D. Nakauchi, N. Kawaguchi, K. Watanabe, and T. Yanagida: Sens. Mater. **35** (2023) 451. https://doi.org/10.18494/SAM4141
21 K. Okazaki, D. Nakauchi, H. Fukushima, T. Kato, N. Kawaguchi, and T. Yanagida: Sens. Mater. **35** (2023) 459. https://doi.org/10.18494/SAM4144
22 D. Yuan, E. G. Víllora, N. Kawaguchi, D. Nakauchi, T. Kato, T. Yanagida, and K. Shimamura: Jpn. J. Appl. Phys. **62** (2023) 010614. https://doi.org/10.35848/1347-4065/aca3e5
23 T. Kunikata, T. Kato, D. Shiratori, D. Nakauchi, N. Kawaguchi, and T. Yanagida: Sens. Mater. **34** (2022) 661. https://doi.org/10.18494/SAM3683
24 T. Kato, D. Nakauchi, N. Kawaguchi, and T. Yanagida: Sens. Mater. **34** (2022) 653. https://doi.org/10.18494/SAM3682
25 Y. Yoshikawa, T. Kato, D. Nakauchi, N. Kawaguchi, and T. Yanagida: Jpn. J. Appl. Phys. **61** (2022) 102001. https://doi.org/10.35848/1347-4065/ac88ab
26 T. Kunikata, T. Kato, D. Shiratori, D. Nakauchi, N. Kawaguchi, and T. Yanagida: J. Mater. Sci.: Mater. Electron. **33** (2022) 2234. https://doi.org/10.1007/s10854-021-07436-7
27 D. Nakauchi, F. Nakamura, T. Kato, N. Kawaguchi, and T. Yanagida: Sens. Mater. **35** (2023) 467. https://doi.org/10.18494/SAM4138
28 H. Kimura, T. Kato, D. Nakauchi, N. Kawaguchi, and T. Yanagida: Sens. Mater. **34** (2022) 691. https://doi.org/10.18494/SAM3687
29 D. Shiratori, H. Fukushima, D. Nakauchi, T. Kato, N. Kawaguchi, and T. Yanagida: Jpn. J. Appl. Phys. **62** (2023) 122227. https://doi.org/10.35848/1347-4065/ac90a4
30 E. Kaewnuam, N. Wantana, Y. Ruangtaweep, M. Cadatal-Raduban, K. Yamanoi, H. J. Kim, P. Kidkhunthod, and J. Kaewkhao: Sci. Rep. **12** (2022) 11059. https://doi.org/10.1038/s41598-022-14833-3
31 H. Fukushima, D. Shiratori, D. Nakauchi, T. Kato, N. Kawaguchi, and T. Yanagida: Sens. Mater. **34** (2022) 717. https://doi.org/10.18494/SAM3691
32 N. Kawaguchi, D. Nakauchi, T. Kato, Y. Futami, and T. Yanagida: Sens. Mater. **34** (2022) 725. https://doi.org/10.18494/SAM3705
33 N. Kawaguchi, K. Watanabe, D. Shiratori, T. Kato, D. Nakauchi, and T. Yanagida: Sens. Mater. **35** (2023) 499. https://doi.org/10.18494/SAM4136
34 Y. Takebuchi, D. Shiratori, T. Kato, D. Nakauchi, N. Kawaguchi, and T. Yanagida: Sens. Mater. **35** (2023) 507. https://doi.org/10.18494/SAM4142
35 H. Kimura, T. Fujiwara, M. Tanaka, T. Kato, D. Nakauchi, N. Kawaguchi, and T. Yanagida: Sens. Mater. **35** (2023) 513. https://doi.org/10.18494/SAM4146
36 H. Masai, and T. Yanagida: Jpn. J. Appl. Phys. **62** (2023) 010606. https://doi.org/10.35848/1347-4065/ac91b8
37 N. Wantana, E. Kaewnuam, Y. Tariwong, N. D. Quang, P. Pakawanit, C. Phoovasawat, N. Vittayakorn, S. Kothan, H. J. Kim, and J. Kaewkhao: Jpn. J. Appl. Phys. **62** (2023) 010602. https://doi.org/10.35848/1347-4065/ac9876
38 H. Fukushima, D. Nakauchi, G. Okada, N. Kawaguchi, and T. Yanagida: J. Mater. Sci.: Mater. Electron. **29** (2018) 21033. https://doi.org/10.1007/s10854-018-0249-9
39 E. V. van Loef, Y. Wang, S. R. Miller, C. Brecher, W. H. Rhodes, G. Baldoni, S. Topping, H. Lingertat, V. K. Sarin, and K. S. Shah: Opt. Mater. **33** (2010) 84. https://doi.org/10.1016/j.optmat.2010.08.013
40 J. Pejchal, C. Guguschev, M. Schulze, V. Jary, E. Mihokova, K. Rubesova, V. Jakes, J. Barta, and M. Nikl: Opt. Mater. **98** (2019) 109494. https://doi.org/10.1016/j.optmat.2019.109494
41 A. Grezer, E. Zych, and L. Kpiński: Radiat. Meas. **45** (2010) 386. https://doi.org/10.1016/j.radmeas.2009.09.014
42 C. Greskovich and S. Duclos: Annu. Rev. Mater. Sci. **27** (1997) 69. https://doi.org/10.1146/annurev.matsci.27.1.69

43 H. Fukushima, D. Nakauchi, T. Kato, N. Kawaguchi, and T. Yanagida: J. Lumin. **250** (2022) 119088. https://doi.org/10.1016/j.jlumin.2022.119088
44 H. Fukushima, D. Nakauchi, T. Kato, N. Kawaguchi, and T. Yanagida: Sens. Mater. **35** (2023) 429. https://doi.org/10.18494/SAM4139
45 H. Fukushima, D. Nakauchi, G. Okada, T. Kato, N. Kawaguchi, and T. Yanagida: J. Alloys Compd. **934** (2023) 167929. https://doi.org/10.1016/j.jallcom.2022.167929
46 E. V. Van Loef, W. M. Higgins, J. Glodo, C. Brecher, A. Lempicki, V. Venkataramani, W. W. Moses, S. E. Derenzo, and K. S. Shah: IEEE Trans. Nucl. Sci. **54** (2007) 741. https://doi.org/10.1109/TNS.2007.896343
47 D. Nakauchi, G. Okada, N. Kawaguchi, and T. Yanagida: Jpn. J. Appl. Phys. **57** (2018) 100307. https://doi.org/10.7567/JJAP.57.100307
48 T. Yanagida, K. Kamada, Y. Fujimoto, H. Yagi, and T. Yanagitani: Opt. Mater. **35** (2013) 2480. https://doi.org/10.1016/j.optmat.2013.07.002
49 T. Yanagida, Y. Fujimoto, T. Ito, K. Uchiyama, and K. Mori: Appl. Phys. Express **7** (2014) 062401. https://doi.org/10.7567/APEX.7.062401
50 R. D. Shannon: Acta Crystallogr., Sect. A: Found. Crystallogr. **32** (1976)751. https://doi.org/10.1107/S0567739476001551
51 Y. Ji, D. Y. Jiang, J. J. Chen, L. S. Qin, Y. P. Xu, T. Feng, and J. L. Shi: Opt. Mater. **28** (2006) 436. https://doi.org/10.1016/j.optmat.2005.04.003
52 T. Yanagida, J. Ueda, H. Masai, Y. Fujimoto, and S. Tanabe: J. Non-Cryst. Solids **431** (2016) 140. https://doi.org/10.1016/j.jnoncrysol.2015.04.033
53 K. Takagi and T. Fukazawa: Appl. Phys. Lett. **42** (1983) 43. https://doi.org/10.1063/1.93760
54 C. L. Melcher and J. S. Schweitzer: IEEE Trans. Nucl. Sci. **39** (1992)502. https://doi.org/10.1109/23.159655
55 W. Chewpraditkul, L. Swiderski, M. Moszynski, T. Szczesniak, A. Syntfeld-Kazuch, C. Wanarak, and P. Limsuwan: IEEE Trans. Nucl. Sci. **56** (2009) 3800. https://doi.org/10.1109/TNS.2009.2033994
56 Q. J. Liu, Z. T. Liu, L. P. Feng, and H. Tian: Physica B **405** (2010) 4032. https://doi.org/10.1016/j.physb.2010.06.051
57 H. Fukushima, D. Nakauchi, N. Kawaguchi, and T. Yanagida: Sens. Mater. **31** (2019) 1273. https://doi.org/10.18494/SAM.2019.2187
58 T. Yanagida: Proc. Jpn. Acad. Ser. B **94** (2018) 75. https://doi.org/10.2183/pjab.94.007